J. Exp. Biomed. Sci. 11 (2005) 129-134

Quantification of Cerebral Blood Flow Measurements by Magnetic Resonance Imaging Bolus Tracking

Byung-Rae Park†

Department of Radiological Science, Catholic University of Pusan, Busan 609-757, Korea

Three different deconvolution techniques for quantifying cerebral blood flow (CBF) from whole brain T2*-weighted bolus tracking images were implemented (parametric Fourier transform P-FT, parametric single value decomposition P-SVD and nonparametric single value decomposition NP-SVD). The techniques were tested on 206 regions from 38 hyperacute stroke patients. In the P-FT and P-SVD techniques, the tissue and arterial concentration time curves were fit to a gamma variate function and the resulting CBF values correlated very well ($CBF_{P\text{-}FT} = 1.02 \cdot CBFp_{\text{-}SVD}$, $r^2 = 0.96$). The NP-SVD CBF values correlated well with the P-FT CBF values only when a sufficient number of time series volumes were acquired to minimize tracer time curve truncation ($CBF_{P\text{-}FT} = 0.92 \cdot CBF_{NP\text{-}SVD}$, $r^2 = 0.88$). The correlation between the fitted CBV and the unfitted CBV values was also maximized in regions with minimal tracer time curve truncation ($CBV_{fit} = 1.00 \cdot CBV_{unfit}$, $r^2 = 0.89$). When a sufficient number of time series volumes could not be acquired (due to scanner limitations) to avoid tracer time curve truncation, the P-FT and P-SVD techniques gave more reliable estimates of CBF than the NP-SVD technique.

Key Words: Bolus tracking, Quantitative cerebral perfusion, Gradient echo EPI

INTRODUCTION

Several groups have reported using MRI bolus tracking to quantitatively measure cerebral blood flow (CBF) and cerebral blood volume (CBV) (Rempp et al., 1994; Ostergaard et al., 1998; Hagen et al., 1999). These techniques acquire a time series of T2*-weighted images after an intravenous bolus injection of an MR contrast agent and measurements of CBF, CBV, and mean transit time (MTT) are made by applying indicator dilution theory (Meier and Zierler, 1954; Zierler, 1962; Axel, 1980). These values can be quantitative (i.e., expressed in absolute units) if the arterial input function (AIF) can be measured and used to deconvolve the tissue curves in the case of CBF or used to normalize the integral of the tissue curves in the case of CBV.

Although the above-mentioned groups all based their techniques on the same theory, significant differences existed in their implementation of this theory. Both fitted the AIF and tissue curves to a gamma variate function and then performed the deconvolution using the Fourier transform (FT) technique, which in this paper is called the P-FT technique where P stands for parametric due to the gamma variate fitting. The reported CBF and CBV values for white matter (WM) and gray matter (GM) either agreed well with values reported from the PET literature or with CBF values measured in the same patients using xenon CT.

Ostergaard et al., 1996, used a nonparametric (NP) single value decomposition (SVD) to perform the deconvolution (i.e., no fitting of curves), called NP-SVD in this paper. Using computer simulations based on a voxel-by-voxel analysis, they showed that the NP-SVD technique estimated CBF relatively independent of the underlying vascular structure and volume compared to techniques that model analytically the actual vascular structure such as an exponential function. When comparing the NP-SVD technique to an NP-FT technique, they showed that the NP-FT technique underestimated CBF at high flow (>35 ml/min/ 100 g) and was biased by the CBV value. Note that they tested an NP-FT technique, meaning that they did not fit the AIF and tissue curves to a gamma variate function but instead

*Received: April 6, 2005
Accepted after revision: April 29, 2005

†Corresponding author: Byung-Rae Park, Department of Radiological Science, Catholic University of Pusan, #9, Bugok 3-dong, Geumjeong-gu, Busan 609-757, Korea.
Tel: 051-510-0583, Fax: 051-510-0588, e-mail: brpark@cup.ac.kr

deconvolved the original curves using the FT. They verified their technique by correlating CBF and CBV measurements from normal volunteers to those from $H_2{}^{15}0$ PET and were able to obtain quantitative MRI values by using an empirical constant that related MRI flow rates in susceptibility contrast units to absolute flow rates measured by PET (Ostergaard et al., 1998).

Since the NP-SVD technique does not fit the data to any analytical functions, the CBF, CBV and MTT measures should theoretically be the least biased. However, the technique used to perform the deconvolution (SVD) is an approximation to the deconvolution operation and bias may be introduced at this step. The purpose of this work was twofold. First, comparisons were made between CBF values calculated using the P-FT and P-SVD techniques to determine if FT deconvolution is significantly different than SVD deconvolution. Second, the CBF and CBV values calculated using the P-FT technique were compared to the corresponding values calculated using the NP-SVD technique to determine if significant differences existed between the two techniques.

MATERIALS AND METHODS

1. MRI protocol

Thirty-eight patients with confirmed stroke (a posteriori) underwent an MRI study within 6 hr of symptoms onset. These patients were selected from a larger population who had undergone the same MRI protocol. All imaging was performed using a 1.5 T GE Signa scanner (GE Medical Systems, Milwaukee, WI) with 5 mm slice thickness, 0.5 mm interslice gap, 24×24 cm^2 field of view (FOV) and 24 slices per volume. A diffusion trace volume (to delineate new infarcts) was calculated from three diffusion weighted volumes with the diffusion gradients applied along each of the x, y, and z directions, respectively, using a spin-echo echo-planar imaging (EPI) sequence (TR = 4500 msec, TE = 95 msec, 128×128 matrix, b = 1000 sec/mm^2, $\delta = 32$ msec and $\Delta = 39$ msec). A single shot gradient echo EPI sequence (128×96 matrix, TR $\times$ 2.3 sec, TE $\times$ 30 msec) was used to perform the bolus tracking, with the sequence started either at the same time or a few seconds after the Gd-DTPA injection. Gd-DTPA (0.1 mmol/kg) was injected at a rate of 10 ml/sec in an antecubital vein by an MRI power injector (Medrad Inc., Pittsburgh, PA) followed by a 30 ml saline flush. Therefore, the duration of the Gd-DTPA bolus was 1.5 sec for a 75 kg patient, and 4.5 sec for the Gd-DTPA bolus plus the saline flush. The entire brain volume was imaged every 2.3 sec for 46 sec after injection of Gd-DTPA (20 volumes total). No smoothing was performed on any of the images. The first acquired bolus tracking volume was used only for registration and display purposes since it was not in steady state magnetization, and time 0 in our study was assigned to the second acquired volume, therefore 43.7 sec was assigned to the 20 th acquired volume.

2. Data processing

All images were transferred to an offline workstation (Sun Ultra 1/200, Sun Microsystems, Mountain View, CA) for processing using programs written in C and IDL (Research Systems, Inc., Boulder, CO). A registration was performed when anatomically drawn contours on the first bolus tracking volume did not match the anatomy of the diffusion images. Patient movement during the acquisition of the 20 bolus tracking volumes was detected by playing a cine loop of the same slice with respect to time. If movement greater than approximately 1 voxel was detected, each bolus tracking volume was registered to the last acquired bolus tracking volume.

MR signal intensity was converted to Gd concentration using the relation $C_m(t) = K \cdot ln\,[S(t)/S_0]$ where $C_m(t)$ is the measured concentration of Gd-DTPA with respect to time, K is a proportionality constant that depends on the magnetic field, type of contrast agent and TE of the imaging sequence, $S(t)$ is the MRI signal intensity with respect to time, and S_0 is the baseline MRI signal before the presence of Gd-DTPA and after a steady-state magnetization has been achieved. We used three images (2 nd, 3 rd, and 4 th acquired bolus tracking volumes) to calculate $S_0 \cdot C_m(t)$ could be calculated on a voxel-by-voxel basis (i.e., to form CBF and CBV maps) as well as a region of interest (ROI) basis.

Indicator dilution theory can be applied to MR bolus tracking images to quantify CBF, CBV, and MTT. When an ideal instantaneous arterial bolus (i.e., a delta function) of Gd-DTPA is the input to a tissue region, the following relation exists between the parameters:

$$\frac{CBV}{CBF} = \frac{\int C(t)dt}{C_{max}} \qquad [1]$$

where $C(t)$ is the concentration of Gd-DTPA in a tissue region and C_{max} is the maximum of this curve. However, an instantaneous arterial bolus is not possible in practice but can be calculated using the relation $C(t) = C_m(t), \otimes^{-1} AIF(t)$ where $C_m(t)$ is the measured tissue curve and $\otimes^{-1}$ represents the deconvolution operation. Absolute CBV can be calculated as

$$CBV = \frac{\kappa}{\rho} \cdot \frac{\int C_m(t)dt}{\int AIF(t)dt} \quad [2]$$

where $\kappa = (1\text{-}HCT_{LV}) / (1\text{-}HCT_{SV})$corrects for the fact that the hematocrit in large vessels (HCT_{LV} was set to 0.45) is larger than the hematocrit of small vessels (HCT_{SV} was set to 0.25) (Rempp et al., 1994) and p is the density of brain tissue (1.04 g/ml) (Axel, 1980). Once C(t) and CBV have been calculated, CBF can be calculated using Eq. [1]. Finally, MTT was calculated using $MTT = CBV/CBF$.

3. Gamma variate fitting

When employing the P-FT and P-SVD techniques, the tissue and AIF curves were fit to a gamma variate function (Rempp et al., 1994; Hagen et al., 1999) using the Levenberg-Marquardt method (Press et al., 1992; Marquart, 1963):

$$AIF_{fit}(t) \text{ or } C_{fit}(t) = -K(X+\Delta)^{\alpha} \cdot e^{-(X+\Delta)/B} \cdot F_{step}(X+\Delta) \quad [3]$$

where $AIF_{fit}(t)$ and $C_{fit}(t)$ are the fitted AIF(t) and $C_m(t)$ curves, respectively, K is a constant, X is the image number, Δ is the delay between image 0 and the arrival of the bolus, α and B are gamma variate parameters, and F_{step} is a step function defined by:

$$F_{step} = \begin{cases} 1 \text{ for } (X+\Delta) \geq 0 \\ 0 \text{ for } (X+\Delta) < 0 \end{cases} \quad [4]$$

The fitting was implemented both on a voxel-by-voxel basis and an ROI basis. To eliminate the effects of recirculation, any time points that were less than 30% of the maximum after the peak of the curves were not used in the fit. For regions with poor bolus passage (i.e., infarcted or penumbra regions), this threshold was adjusted by the user until the X^2 value was within $\pm 10\%$ of the X^2 value of the healthy mirror region. If this was not possible due to very poor bolus passage (and hence a noisy signal), these regions were excluded from the study.

4. FT deconvolution

After fitting the AIF(t) and $C_m(t)$ curves to the gamma variate function, the curves were extrapolated to the scanner (60 time points or 138 sec) to allow a smooth transition to a Gd-DTPA concentration. Zero-padding was used to elongate the $AIF_{fit}(t)$ and $C_{fit}(t)$ curves to the next power of 2 (in this case only 4 zeros were added to make the total number of time points 64) before performing the deconvolution using the Fourier transform F:

$$C(t) = F^{-1}\left[\frac{F\{C_{fit}(t)\}}{F\{AIF_{fit}(t)\}}\right] \quad [5]$$

where F^{-1} represents the inverse Fourier transform.

5. SVD deconvolution

The AIF can also be deconvolved from the tissue curve using algebraic techniques that linearize the deconvolution operation as was done. For details of this implementation, the reader is referred to reference (Ostergaard et al., 1996). In short, the values for the AIF and $C_m(t)$ curves can be written in vector notation as $C = AIF^{-1} \cdot Cm$, where C represents the matrix of the deconvolved C(t) curve. This equation can be solved using the SVD technique, whereby the matrix AIF is decomposed into three matrices $AIF = U \cdot W \cdot V^T$ (Press et al., 1992). The inverse of AIF can be calculated as $AIF^{-1} = V \cdot [diag(1/w_j)] \cdot U^T$, where $[diag(1/w_j)]$ represents the reciprocals of the diagonal elements of W. When calculating AIF^{-1}, problems arise when W contains singular values (i.e., $w_j = 0$ or is close to 0) and will cause the curve C(t) to oscillate. Therefore, Ostergaard et al., 1996, used a cutoff threshold to eliminate these oscillations, and set this threshold to be 15~20% of the maximum value in the diagonal matrix W. We used a cutoff threshold of 15% except for data acquired from five patients where cutoffs of 40, 60, and 80% were also used to determine the effect this had on the CBF calculation.

6. Image analysis

Qualitative maps of the CBV and MTT in brain tissue were calculated by integrating the $C_m(t)$ curves and calculating the first moment of the $C_m(t)$ curves, respectively, on a voxel-by-voxel basis. The average and standard deviation

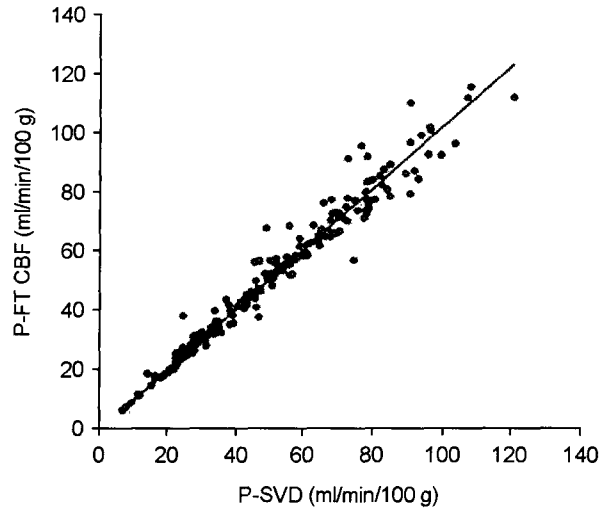

Fig. 1. Comparison of CBF calculated with the P-FT technique and SVD technique for all 206 ROIs. The linear regression equation was $CBF_{P\text{-}FT} = 1.02 \cdot CBFp_{\text{-}SVD}$ with $r^2 = 0.96$.

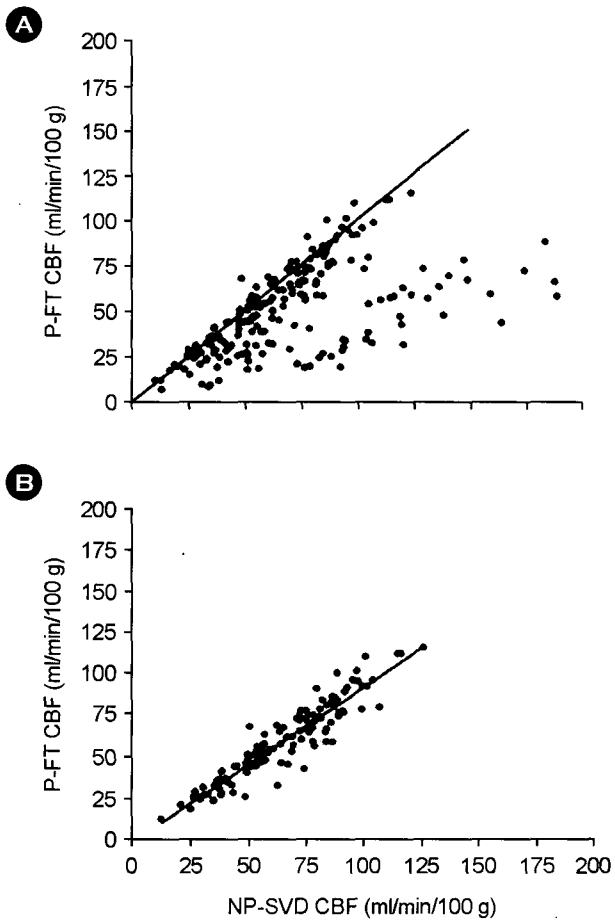

Fig. 2. A: P-FT calculated CBF compared to NP-SVD CBF for all 206 regions displayed with the line of identity. **B:** Same as in a except only a subset of the regions was plotted. The linear regression line is also displayed and the equation was $CBF_{P\text{-}FT} = 0.92 \cdot CBF_{NP\text{-}SVD}$ with $r^2 = 0.88$.

of the CBV volume were calculated, and those voxels that had a CBV value > 2SD from the average were excluded from further analysis since these voxels were most likely large vessels. Six 3D ROIs were drawn for each patient. Two ROIs were drawn on the contralateral side with respect to the infarcted areas in the thalamus and the white matter in the centrum semiovale on the first volume of the bolus tracking images. A trained radiologist outlined the hyperintense signal area (corresponding to the infarct) on the diffusion trace volume, and this ROI was called the infarcted ROI, and the same radiologist placed an ROI on the abnormally long (with respect to the contralateral side) mean transit times on the calculated MTT volume. The difference between this ROI and the infarcted ROI was called the penumbra ROI. The final two ROIs were the contralateral mirror ROIs of the infarcted and penumbra ROIs. Quantitative values of CBF, CBV, and MTT were calculated for all ROIs using the three different techniques: P-FT, P-SVD, and NP-SVD using the exact same AIF and tissue ROIs. Linear regression analysis was used to quantify correlation between data and a two-tailed two sample *t*-test assuming unequal variances was used to test for significant differences between groups. A *P* value of 0.05 was considered significant.

RESULTS

In data from one patient, no abnormal hyperintense signal was seen on the trace diffusion volume, and thus no infarcted ROI and its corresponding mirror ROI could be drawn. In data from eight patients, no abnormal MTT regions were seen on the calculated MTT volume, and thus no penumbra ROIs and their corresponding mirror ROIs existed for these patients. Three infarcted regions and one penumbra region were excluded due to inadequate bolus passage, and hence a poor gamma variate fit. The cutoff threshold for the gamma variate fit had to be adjusted by the user for 13 infarct and penumbra regions. A total of 206 ROIs were analyzed and compared. Fig. 1 shows the comparison between the P-FT and the P-SVD calculated CBF values for all 206 regions. Note the excellent agreement between these two techniques and no significant difference was found between the two groups (P=0.66). Fig. 2a shows the comparison between the P-FT and NP-SVD calculated CBF values for

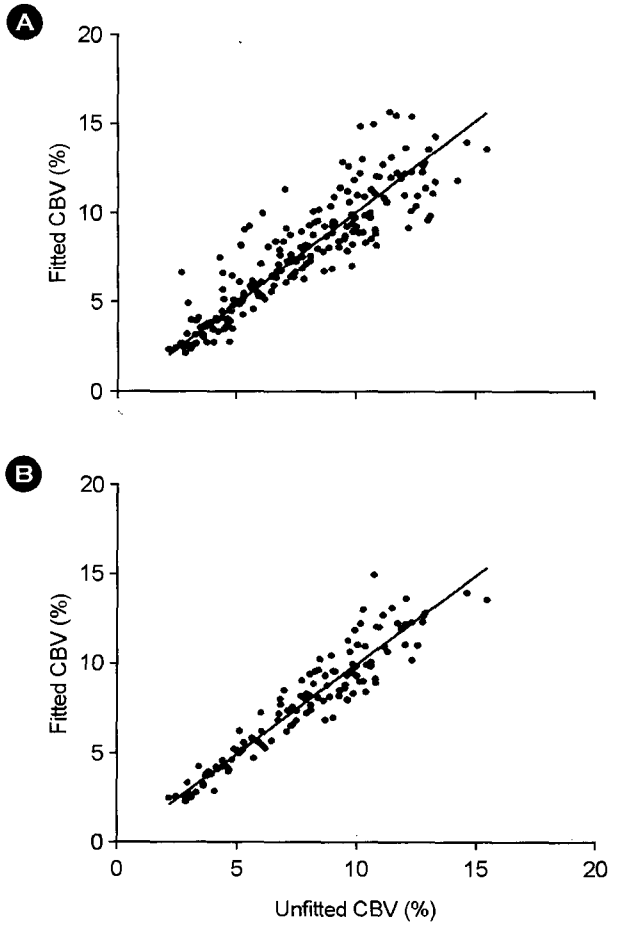

Fig. 3. A: Fitted CBV values versus unfitted CBV values for all 206 ROIs. The linear regression equation was $CBV_{fit} = 1.01 \cdot CBV_{unfit}$ with $r^2 = 0.78$. **B:** Same as in a except only a subset of the regions was compared. The linear regression equation was $CBV_{fit} = 1.00 \cdot CBV_{unfit}$ with $r^2 = 0.89$.

all 206 regions. The correlation coefficient was 0.17 and there was a significant difference between the two groups ($P<0.0001$), with the NP-SVD CBF values generally being larger than the P-FT CBF values. Note that two distinct groups are present in this graph. A subset of the 206 regions was made by only taking those regions where the peak of the AIF(t) occurred before 13.8 see and the peak of the tissue $C_m(t)$ occurred before 18.4 see, thus eliminating those tissue curves that had severe tracer time curve truncation. Fig. 2b shows the comparison for this subset of 123 regions and there was no significant difference between these two groups ($P=0.12$). Fig. 3a shows the fitted CBV values versus the non-fitted CBV values for all 206 regions. No significant difference between these two groups ($P=0.52$) was found. Fig. 3b shows the same graph for the subset of 123 regions, and there was also no significant difference between these two groups ($P=0.99$). Note that the correlation coefficient increased when the subset of regions were compared.

Table 1. Comparison of calculated NP-SVD CBF values (in ml/min/100 g) for the WM ROI and the infarcted ROI using different cutoff threshold

Region	Patient	P-FT	NP-SVD (0.15)	NP-SVD (0.40)	NP-SVD (0.60)	NP-SVD (0.80)
WM	1	26.2	29.0	32.4	25.5	9.5
	2	28.9	37.5	32.9	31.2	12.3
	3	26.0	51.6	41.8	31.6	21.9
	4	28.9	64.0	44.5	29.5	13.0
	5	24.9	39.3	32.5	26.9	14.2
Infarct	1	12.1	39.0	26.1	23.7	10.9
	2	18.9	92.9	50.0	36.9	14.4
	3	31.1	55.5	46.9	51.1	41.9
	4	19.5	79.4	53.0	33.4	15.4
	5	7.3	13.8	12.1	17.9	17.9

The calculated delay for the P-SVD technique ranged from 0 to 13.8 see, with the latter occurring in an infarcted region, while the calculated delay for the NP-SVD technique ranged from 0 to 6.9 see with the latter value corresponding to the same infarcted region as the maximum delay calculated using the P-SVD technique. The P-SVD delay was 0 see for 60% of the 206 regions, while the NP-SVD delay was 0 see for 98% of the regions.

Finally, Table 1 shows the effect of the cutoff threshold when calculating the NP-SVD CBF values from five patients for the WM and infarct ROIs whose regions had significant truncation. Note that no single threshold value consistently gave the most similar result to the P-FT CBF value, suggesting that either truncated ROI curves cannot be used for NP-SVD CBF calculation or that an adaptive threshold must be used.

DISCUSSION

The CBF values calculated using the P-FT and P-SVD technique were in excellent agreement demonstrating that FT and SVD deconvolution are essentially equivalent when the same curves are deconvolved. The P-FT and NP-SVD CBF values only correlated well when tracer time curves with minimal truncation were compared, and in this subset of regions the P-FT CBF values were on average 8% lower than the NP-SVD CBF values. The fitted versus unfitted

CBV values were also in better agreement in this same subset of regions. Although the fitted and unfitted CBV values for all 206 regions were not significantly different, the correlation coefficient did increase when the subset of regions with minimal tracer time curve truncation was used for the comparison. This is probably due to the fact that if the AIF curve is measured with no truncation (or at least less truncation than the tissue curve) and if the tissue curve has been truncated, the unfitted CBV value will be underestimated (see Eq. [2]). Tracer time curve truncation is less of a problem when using the fitted curves since only the initial bolus passage is used and not the tracer recirculation. When using the minimum X^2 value to determine the delay for the P-SVD and NP-SVD techniques, the P-SVD techniques showed a delay different from 0 sec in 40% of the 206 regions, while for the NP-SVD technique only 2% of the regions showed a delay different from 0 sec. This difference is probably due to the fact that in the case of the P-SVD technique, the data have been denoised (i.e., fitted to a gamma variate function), there by making the X^2 function noiseless as well, and a minimum can easily be found, whereas the X^2 function for the NP-SVD was noisy, making it difficult to find the true minimum. Smoothing the images themselves may allow a better estimation of the delay when using the NP-SVD technique. Poor estimation of the delay may also be another reason why the NP-SVD CBF values were on average larger than the P-FT CBF values.

In conclusion, an excellent correlation was found between the CBF values calculated using the P-FT and the P-SVD techniques. When truncation in the tracer time curves was minimized, a good correlation was also found between P-FT CBF and NP-SVD CBF values, although the P-FT CBF values were on average 8% lower. Finally, CBV values calculated from fitted curves were not significantly different from those calculated from the unfitted curves, but minimizing tracer curve truncation increased the correlation between the two sets of CBV values.

REFERENCES

Axel L. Cerebral blood flow determination by rapid-sequence computed tomography. Radiology 1980. 137: 679-686.

Hagen T, Bartylla K, Piepgras U. Correlation of regional cerebral blood flow measured by stable xenon CT and perfusion MRI. J Comp Assist Tomogr. 1999. 23: 257-264.

Marquart DW. An algorithm for least squares estimation of non-linear parameters. J Soc Indust Appl Math. 1963. 11: 431-441.

Meier P, Zierler LL. On the theory of the indicator-dilution method for measurement of blood flow and volume. J Appl Phys. 1954. 6: 731-744.

Ostergaard L, Johannsen P, Host-Poulsen P. Cerebral blood flow measurements by magnetic resonance imaging bolus tracking: comparison with [^{15}O]H_2O positron emission tomography in humans. J Cereb Blood Flow Metab. 1998. 18: 935-940.

Ostergaard L, Sorensen AG, Kwong KK, Weisskoff RM. High resolution measurement of cerebral blood flow using intravascular tracer bolus passages. Part II: experimental comparison and preliminary results. Magn Res Med. 1996. 36: 726-736.

Ostergaard L, Weisskoff RM, Chesler DA, Gyldensted C. High resolution measurement of cerebral blood flow using intravascular tracer bolus passages. Part I: mathematical approach and statistical analysis. Magn Res Med. 1996. 36: 715-725.

Press WH, Teukolsky SA, Vetterling WT, Flannery BT. Numerical recipes in C. The art of scientific computing, 2nd ed. 1992. Cambridge: Cambridge University Press. UK.

Rempp KA, Brix B, Wenz F, C. R. Becker CR. Quantification of regional cerebral blood flow and volume with dynamic susceptibility contrast-enhanced MR imaging. Radiology. 1994. 193: 637-641.

Zierler KL. Theoretical basis of indicator-dilution methods for measuring flow and volume. Circ Res. 1962. 10: 393-407.